

Star-forming Regions in the Small Magellanic Cloud Multi-wavelength Properties of Stellar Complexes

E. Livanou and I. Gonidakis

Department of Astrophysics Astronomy & Mechanics, Faculty of Physics, University of Athens, GR-157 83 Athens, Greece

E. Kontizas

Institute for Astronomy and Astrophysics, National Observatory of Athens, P.O. Box 20048, GR-118 10 Athens, Greece

U. Klein

Argelander-Institut der Universität Bonn, Auf dem Hügel 71, 53121, Bonn, Germany

M. Kontizas

Department of Astrophysics Astronomy & Mechanics, Faculty of Physics, University of Athens, GR-157 83 Athens, Greece

D. Kester

SRON, Netherlands Institute for Space Research, P. O. Box 800, 9700 AV Groningen

Y. Fukui and N. Mizuno

Department of Astrophysics, Nagoya University, Chikusa-ku, Nagoya 464-8602

and

P. Tsalmantza

Department of Astrophysics Astronomy & Mechanics, Faculty of Physics, University of Athens, GR-157 83 Athens, Greece

ABSTRACT

We trace the star formation regions in the SMC and study their properties. The size and spatial distribution of these regions is found to support the hierarchical scenario of star formation, whereas, the evaluation of their intensity, contributes to the understanding of the various stages of star formation. Their

connection to the LMC-SMC close encounter, about $(0.9 - 2) \times 10^8$ years ago, is investigated as well. The SMC, being almost edge-on, does not easily reveal these areas, as is the case with the LMC. However, a study through multi-wavelength images such as optical, IR and radio has been proved very useful. A selection of areas, with enhanced 60 and 100- μm infrared flux and emission in all IRAS bands, identifies the star forming regions. All of the identified regions are dominated by early-type stars and considering their overall size (increasing order) a total of 24 aggregates, 23 complexes, and 3 super-complexes were found. We present their coordinates, dimensions, and IR fluxes. Moreover, we correlate their positions with known associations, SNRs, and HII regions and discuss their activity.

Subject headings: galaxies: stellar content — Magellanic Clouds — stars: formation

1. INTRODUCTION

The Magellanic Clouds, being so close to our galaxy, are the most appropriate example of galaxies in order to study star formation in large scale, and due to their proximity, there are data available in various wavelength regimes. Moreover, the Magellanic Clouds and the Milky Way form an interacting system of galaxies, with tidal forces having significant effects on triggering star formation events.

In a previous paper (Livanou et al. 2006), we studied the connection between various tracers of star formation in the LMC, using different wavelength regimes. In the present paper we conduct an investigation of the SMC, based upon similar data. A distance of 63 kpc is used throughout; however, owing to the large depth of the SMC along the line of sight (Mathewson et al. 1988; Hatzidimitriou & Hawkins 1989), we shall account and correct for this whenever necessary.

Star complexes are the largest and oldest objects among the various size stellar groupings, which start from the multiple stars. The younger and smaller clusters are always within the older and the larger ones. This hierarchy is similar to one observed in the interstellar gas distribution and, in fact, is the result of the latter. Sometimes a galaxy hosts some very bright complexes, which consist of OB-associations and HII regions. They were called long ago the superassociations and represent the local starbursts (Efremov 2004).

Recently, N-body models for tidal interactions showed that the star formation rate in the SMC has been strongly enhanced by the tidal encounters with the LMC that occurred 1.5 Gyr (14 kpc separation) and 0.2 Gyr (7 kpc separation) ago, by a factor of about 3-4.

Interestingly, in these simulations the peak of the star formation rate occurs 200-300 Myr after the first encounter event, so that the star formation rate may still be rising at the present epoch, 200 Myr after the second interaction (Yoshizawa & Noguchi 2003). It is then reasonable to attempt tracing the effect of this enhancement on the current appearance of the SMC.

Maragoudaki et al. (2001) have studied the spatial distribution of the SMC stellar population according to their age, based on optical data. They concluded that the old stellar population shows a rather regular and smooth distribution, which is typical for a spheroidal body, while the younger stellar component is highly asymmetric and irregular, probably due to the severe impact of its close encounter with the LMC some 0.2-0.4 Gyr ago. In particular, the wing and the tail structures are already evident at $(3.4 - 4.0) \times 10^8$ yr, while the new generations of stars appear mainly along the northeast-southwest direction forming the bar. The bar becomes prominent at an age of about $(1.2 - 3.0) \times 10^7$ yr and hosts all stars with age less than 8×10^6 yr, showing how important the recent star formation is for the morphology of the SMC and giving us an indication of where star-forming, even starburst, regions are expected to be detected.

Star forming regions have been found in both Clouds (Maragoudaki et al. 1998, 2001) to include smaller regions with enhanced star formation activity, supporting the hierarchical scenario of large scale star formation process (Efremov & Elmegreen 1998). Ranking them by increasing size, we use the terms: aggregates, complexes and supercomplexes. Considering the intensity of their star formation activity we use the terms: starburst regions and active regions, based on the criteria set by Livanou et al. (2006) for the LMC. Moreover a comparison with LMC reveals that the relevant frequency of the same size structures in the MCs is similar, independently of LMCs larger size. However, star formation is considerably enhanced in the LMC, probably due to higher total mass, H_2 abundance and metallicity. Throughout this work we study the large scale star formation in the SMC. We investigate the criteria of detection of star forming regions and evaluate the intensity of star formation activity in each one and compare with LMC.

In Sect. 2 the observational material is presented. In Sect. 3 we describe how the starforming regions are selected in images at 60 and 100 μm . We estimate their dimensions, rank them by size (aggregates, complexes and super-complexes) and compare with those in optical and radio data. In Sect. 4 the intensity of activity of the selected starforming regions is discussed and their characteristics are given.

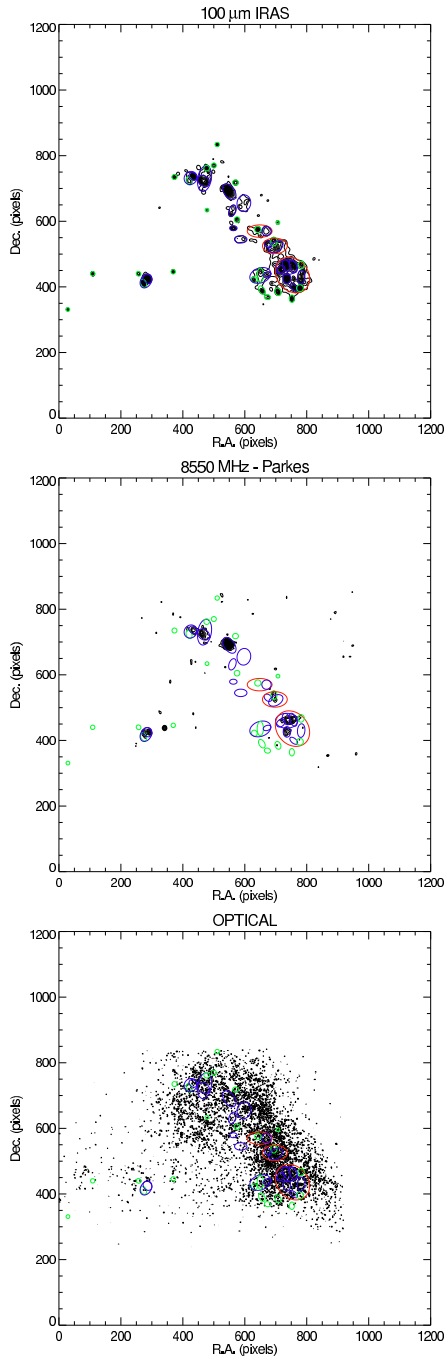


Fig. 1.— Identified star forming regions and their correlation with emission in three different regions of the spectrum (IRAS 100 μm , Parkes 8550 MHz and optical star counts). Red ellipses indicate the super-complexes, blue is for complexes, and green for aggregates.

2. OBSERVATIONAL MATERIAL

In the optical domain, we used the direct photographic plates in U, V and I of the SMC, taken with the 1.2-m UK Schmidt Telescope. The plates that cover an area of $6^{\circ}5 \times 6^{\circ}5$, centred at $\alpha = 01^{\text{h}}07^{\text{m}}22^{\text{s}}.8$, $\delta = -74^{\circ}44'00''.1$ (J2000), were digitized by the fast measuring machine SuperCosmos, providing us with catalogues of detected stars and their corresponding CMDs (Maragoudaki et al. 2001). Based on these data, we created star count images of main-sequence stars for different magnitude slices and pixel sizes, plotting iso-pleth contour maps in order to trace stellar concentrations. The optimum result was achieved for a 750×750 pixel image with pixel sizes corresponding to 9.53 pc. The mean value m and standard deviation σ of the background star density were calculated as the average of four relatively empty regions in the star count image. For the image of the brightest main sequence stars ($13^{\text{m}}.5 < m < 13^{\text{m}}.83$), the minimum contour level was set at $m + 3\sigma$ above the mean background density and the step between different contours was set at 1σ .

We also used the 12, 25, 60, and 100 μm IRAS images by Bontekoe et al. (1999) to produce the infrared isodensity contours of the SMC. They were reconstructed by the HIRAS program using the Pyramid Maximum Entropy Method (Bontekoe et al. 1994). The 1024×1024 images are centred at $\alpha = 01^{\text{h}}00^{\text{m}}54.98^{\text{s}}$ and $\delta = -72^{\circ}54'47''$ (J2000), covering a $4^{\circ}3 \times 4^{\circ}3$ field of view, corresponding to a pixel size of 4.48 pc. For each frame, the mean background value m and standard deviation σ were calculated by the four rather clean corner areas. The plotted contours have 1σ steps over the $m + 3\sigma$ value.

Ionized gas is prominent in star forming regions and its emission stands out clearly in the radio domain. Therefore, we used the 8550 MHz radio continuum map published by (Haynes et al. 1986). The observation was carried out in 1988 November using the Parkes 64-m radio telescope over a 400 MHz bandwidth. Sources with known flux density and position were also observed and used as calibrators. The resulting 201×151 pixel map, centred at $\alpha = 00^{\text{h}}56^{\text{m}}41^{\text{s}}.4$ and $\delta = -72^{\circ}43'47''.6$ (J2000), covers a $3^{\circ}5 \times 2^{\circ}5$ field of view, corresponding to a pixel size of 28.27 pc.

3. DETECTION OF STARFORMING REGIONS

3.1. Selection

The selection of the starforming regions in the SMC was not as straightforward as that in the LMC (Livanou et al. 2006). The optical image is not the most appropriate to identify star-forming regions since the main body of the SMC, appearing almost edge-on, absorbs a

significant amount of the optical light. The radiation from hot young stars is absorbed by dust grains, which heat up and re-emit the energy in the infrared. Especially FIR luminosity is found to be a good indicator of star formation activity. It is known that the flux in 60, and 100 μm characterizes the FIR luminosity of a region. The total far-infrared luminosity is:

$$F_{FIR} = C(60/100) \times 1.26 \times 10^{-14} \times (2.58F_{60} + F_{100})Wm^{-2} \quad (1)$$

where $C(60/100)$ is the color correction dependent on the fitted temperature (Cataloged Galaxies and Quasars Observed in the IRAS Survey, 1985) (Lonsdale et al. (1985); Helou et al. (1988); Lehnert & Heckman (1995)). Thus the intensity of star formation is well represented from the images at 60 and 100 μm . Almost all of the regions of enhanced infrared luminosity, can be identified in all four IRAS images, but most of them have been found systematically smaller at 12 and 25 μm , so we did not use them for our final results. We therefore compared the images at 60 and 100 μm to decide for the final selection and size of the adopted regions. All selected regions are found in both maps with similar sizes (less than 10% difference), thus we could choose either to reveal the borders of the starforming regions. We selected areas with increased 60 and 100- μm infrared flux, which show emission in all IRAS images and resulted in 50 star forming regions (Fig.1 top). The calculated emission of each area in the four IRAS wavebands can be seen in Table 2.

3.2. Sizes

For the size classification of the starforming regions we adopted the values given by Maragoudaki et al. (1998). *Aggregates* are groupings with sizes between 150 and 300 pc, *complexes* range between 300 and 1000 pc and *super-complexes* exceed 1000 pc in diameter, which in our case is set as the major axes of the fitted ellipses. It has to be emphasized that all large structures are found to include smaller. In an attempt to estimate the sizes of these areas, ellipses were fitted to the structures in the 100- μm IRAS image, such as to resemble the structure of each area in the best possible way. However, the edge-on orientation of the SMC required projection corrections to be taken into account. After applying these corrections, 24 aggregates, 23 complexes, and 3 super-complexes were revealed. Fig. 1 shows these regions overplotted on the maps at 100 μm , 8550 MHz and the optical, with green ellipses indicating aggregates, blue corresponding to complexes, and red depicting super-complexes. From the correlation with the optical image of the brightest main sequence stars, we infer the age of the stellar content. The age of this stellar population is younger than 8×10^6 yr (Maragoudaki et al. 2001), giving evidence of being a result of the most recent encounter of SMC and LMC about $(0.9 - 2) \times 10^8$ years ago (Gardiner & Noguchi 1996).

4. ACTIVITY OF STARFORMING REGIONS

Lehnert & Heckman (1995) found that IR-“warm” ($F_{60}/F_{100} \geq 0.4$) and IR-“bright” ($F_{60} \geq 5.4$ Jy) galaxies show strong evidence of forming massive stars at unusually high rates. Thus if any of the detected star forming regions was found with $F_{60}/F_{100} \geq 0.4$ and $F_{60} \geq 5.4$ Jy, it could be considered as a region of enhanced star formation activity. It could even be characterized as starburst if it also had excess of 8550 MHz emission (Livanou et al. 2006). The correlation of the groupings with the Lehnert & Heckman (1995) criterion can be seen in Fig. 2. It is apparent that 8 regions are clearly separated relatively to the rest, occupying the left part of the diagram. However, none of the groupings have F_{60} above the 5.4 Jy threshold.

The stage of evolution of the regions can be estimated by the 8550 MHz map, where enhanced emission reveals areas of on-going star formation, since it reflects mainly thermal emission from ionized gas. Col. 10 of Table 1 indicates the existence or not of 8550 MHz emission, after correlation of the detected star forming regions with the 8550 MHz map. The initial radio map had different pixel size and field of view from the IRAS images. A scaling was performed in all images in order to have the same characteristics, therefore the final images are identical in terms of their sizes and angular resolution. However, there are areas that are not commonly contained in all the images used here, since the observations in the four different wavebands (radio continuum, FIR, optical) have different coverages; such areas are indicated with ‘n/a’ in Table 1 and 3. Apart from the stellar grouping *A2*, which is outside the radio continuum map, the other 7 regions are strongly correlated with the 8550-MHz emission.

Although all eight groupings are correlated with areas where very bright stars are located (see Fig. 1 - optical), none of these eight regions exhibit any increased formation of high-mass stars according to the Lehnert & Heckman (1995) criterion. Contrary to the LMC, where 13 such regions were found, “starburst regions” in the SMC were not identified. The 50 stellar groupings listed here are “active complexes” with clear indications for eight of them showing more intense activity of star formation.

Finally, starbursts are expected to have a larger amount of SNRs, HII regions, and stellar associations than normal galaxies. Fig. 3 shows the distribution of stellar associations, SNRs and HII regions, plotted over the IRAS 100- μ m image. Results can be seen in Cols. 7, 8 and 9 of Table 1. The catalogue compiled by Bica & Schmitt (1995) is used to cross match the areas of interest with these objects. The detected starforming regions obviously contain a larger number of SNRs, HII regions, and stellar associations than their environment. This fact strengthens our claim that star formation is enhanced in these areas.

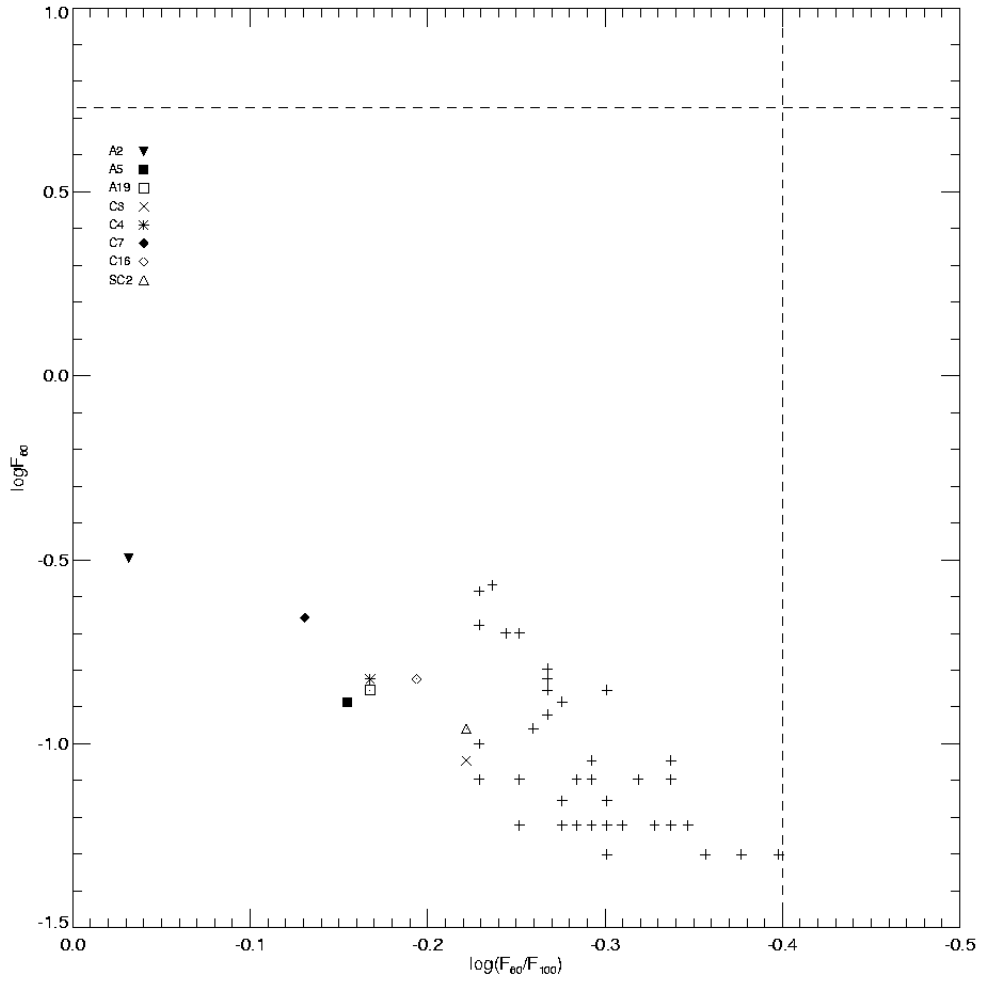


Fig. 2.— Flux at $60 \mu\text{m}$ versus the colour $\log(F_{60}/F_{100})$ for the SMC detected regions. The eight regions indicated by different symbols, are more active in star formation than the rest.

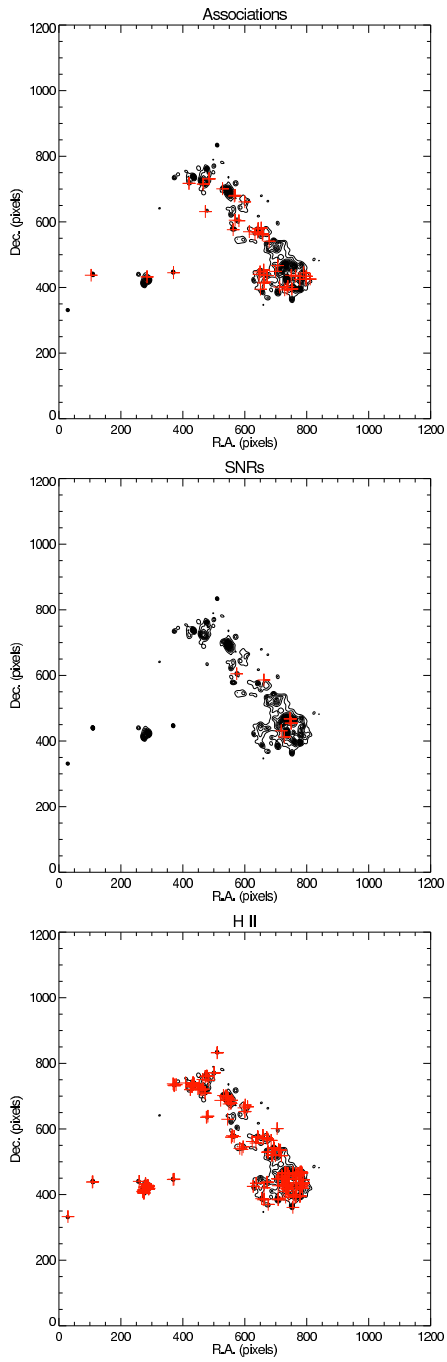


Fig. 3.— Correlated associations, SNR, and HII regions plotted over the $100\ \mu\text{m}$ IRAS image.

5. COMPARISON OF THE LMC WITH THE SMC

Fig. 4 shows a comparison between the two Magellanic Clouds. The left panel shows the frequency distribution of the IR luminosities at $100\ \mu\text{m}$, with solid lines for the SMC and dashed for the LMC. The right panel shows the frequency distribution for each kind of stellar grouping identified in each galaxy, where black bars represent the LMC and grey the SMC. LMC is almost face-on so there are no intrinsic differences in the luminosity due to distance. For the SMC corrections due to depth have to be considered.

Mathewson et al. (1988) studied the distances of 61 Cepheids along the SMC bar, revealing a three dimensional perspective for the SMC. The distribution of these Cepheids showed that the northeastern section of the bar is 10-15 kpc closer than the southern section. Thus, luminosities in the northeast, the central and the southwest part of the bar may vary up to 12.3, 6.25, and 9.75 % respectively. However, in some extreme cases this factor may extend up to 50 %.

It appears that the relative frequencies of aggregates, complexes, and super-complexes in both galaxies are almost the same, while the star-forming activity differs significantly. The histograms of their $100\text{-}\mu\text{m}$ luminosities (adopted at 63 kpc) were fitted with Gaussians such as to reveal similarities in these distributions. Apart from a shift of their centres, the Gaussians reflect similar properties. The best fit for the SMC produces a Gaussian centred at $\log L_{100}=5.51$ (in units of L_{\odot}), with an amplitude of 0.349 ± 0.015 and a standard deviation of 0.60 ± 0.03 , while for the LMC the center is located at $\log L_{100}=6.56$, with an amplitude of 0.307 ± 0.025 and a standard deviation of 0.648 ± 0.024 . Within the range defined by the errors, shapes of these Gaussians can be considered as identical. The shift is not significantly affected by the depth, as explained above and can be a result of the known difference in the colour-corrected flux F_{100} for the SMC is 15.51×10^3 Jy and 190.6×10^3 Jy for the LMC (Rice et al. 1988).

6. CONCLUSIONS

We have identified the large scale star-forming regions in the SMC in order to investigate its activity. This study is associated to the past interaction history of the LMC and SMC, which had a close encounter about $(0.9 - 2) \times 10^8$ years ago. For the identification of the star-forming regions a selection was based upon an increased 60 and $100\text{-}\mu\text{m}$ infrared flux and then compared to the optical and radio image. Ranking them by increasing order of size, we detected 24 aggregates, 23 complexes, and 3 super-complexes. It has to be emphasized that all large structures include smaller ones, supporting the hierarchical scenario of star

formation in large scales.

All of the identified regions are dominated by early-type stars. These stars are found to be younger than $\sim 8 \times 10^8$ years old and thus are believed to be formed as a consequence of the LMC-SMC close encounter.

In order to classify these regions in terms of their activity we compare their IR fluxes with those of other galaxies, in particular starburst galaxies. We find none of the star forming regions detected here to fulfill the criteria of starburst regions contrary to what is observed in the LMC. However 8 of the star forming regions are more active than the rest.

By inspecting optical and radio images of the SMC, we have assessed any correlation with known associations, SNRs and HII regions. The southern-most part of the bar of the SMC appears to be the most diverse in terms of star formation activity, which is probably connected with its large depth along the line of sight. For the northern part of the bar we conjecture that star formation has started in the recent past, mainly inferred from the lack of SNRs and the low number of stellar associations.

If this activity in both galaxies is considered to be triggered, during their recent close encounter, the intensity of this activity is evidently much higher in the LMC than in the SMC. Could this reflect the difference in the total mass, in gas or metallicity between these galaxies? Was the gas removed from the less massive galaxy (SMC) more easily preventing high star formation activity?

7. ACKNOWLEDGMENTS

The authors wish to thank the General Secretariat of Research and Technology for financial support. The project is co-funded by the European Social Fund and National Resources-(EPEAEK II) PYTHAGORAS II. U. Klein is very grateful to the Department of Astrophysics, Astronomy & Mechanics at the University of Athens for the kind hospitality.

Table 1: Star forming regions of the SMC and their properties.

Star forming region	RA (J2000) h m s	DEC (J2000) deg m s	RA Pixels	Dec Pixels	Dimension (pc)	No. of Associations	No. of SNRs	No. of HII regions	8550 MHz
A1	1:29:27	-73:33:50	29	331	160.52	0	0	1	n/a
A2	1:24:09	-73:08:54	109	440	187.27	1	0	2	n/a
A3	1:15:39	-73:11:48	257	440	191.90	0	0	1	-
A4	1:14:50	-73:19:17	273	411	266.62	0	0	12	✓
C1	1:14:21	-73:17:39	281	418	505.38	1	0	23	✓
C2	1:14:02	-73:15:58	286	425	377.06	1	0	12	✓
A5	1:09:11	-73:11:39	369	447	187.27	1	0	2	✓
A6	1:08:26	-71:59:28	373	735	214.02	0	0	5	-
A7	1:05:55	-72:02:46	420	723	257.37	1	0	2	✓
C3	1:05:38	-72:00:33	425	732	551.47	1	0	9	✓
C4	1:05:12	-71:59:20	433	737	338.64	0	0	7	✓
C5	1:03:23	-72:02:57	467	723	508.85	2	0	5	✓
C6	1:03:13	-72:01:12	470	730	619.09	2	0	14	✓
A8	1:02:49	-71:53:13	477	762	240.78	0	0	4	✓
A9	1:02:49	-72:25:13	478	634	160.52	1	0	3	-
A10	1:01:35	-71:51:15	500	770	214.02	0	0	2	-
A11	1:00:60	-71:35:15	511	834	187.27	0	0	2	-
C7	0:58:53	-72:11:12	550	690	588.40	3	0	13	✓
C8	0:58:18	-72:25:41	560	632	331.69	0	0	1	-
C9	0:58:06	-72:38:55	563	579	321.04	1	0	4	-
A12	0:57:48	-72:04:09	570	718	241.47	0	0	0	-
A13	0:57:27	-72:32:23	575	605	240.78	2	1	0	-
C10	0:56:43	-72:47:20	587	545	535.06	0	0	3	-
C11	0:56:17	-72:19:47	597	655	591.74	1	0	5	-
A14	0:54:02	-73:17:49	631	422	242.92	0	0	1	-
A15	0:53:40	-72:39:30	642	575	267.53	2	0	2	-
SC1	0:53:20	-72:40:42	648	570	1070.12	7	1	9	✓
C12	0:52:58	-73:14:25	650	435	902.74	6	0	4	-
A16	0:52:58	-73:14:10	650	436	267.53	2	0	2	-
A17	0:52:35	-73:25:37	655	390	292.28	1	0	3	-
C13	0:52:06	-72:40:31	670	570	401.30	1	0	3	-
C14	0:51:42	-73:13:28	672	438	329.35	1	0	1	-
A18	0:51:29	-73:30:42	673	369	259.47	0	0	1	-
C15	0:51:44	-72:50:27	675	530	333.77	0	0	2	-
A19	0:50:41	-72:48:16	694	538	267.53	0	0	2	✓
SC2	0:50:29	-72:51:29	697	525	1070.12	1	0	12	✓
C16	0:50:18	-72:52:12	700	522	615.87	0	0	7	✓
A20	0:50:06	-72:33:38	707	596	160.52	0	0	1	-
A21	0:49:32	-73:26:20	707	385	253.52	0	0	3	✓
C17	0:49:12	-73:09:14	716	453	354.85	0	0	4	✓
C18	0:48:13	-73:06:01	734	465	347.19	0	1	7	✓
C19	0:48:08	-73:07:15	735	460	963.11	1	2	17	✓
C20	0:47:58	-73:15:43	736	426	321.04	0	0	12	✓
A22	0:46:50	-73:30:58	752	364	214.03	0	0	1	-
SC3	0:46:58	-73:12:58	754	436	1479.86	14	4	56	✓
C21	0:46:57	-73:06:12	756	463	353.92	0	2	8	✓
C22	0:46:36	-73:22:09	758	399	328.43	1	0	3	-
A23	0:45:26	-73:22:35	778	396	294.28	0	0	2	✓
A24	0:45:28	-73:04:48	782	467	263.93	0	0	7	✓
C23	0:45:20	-73:14:02	782	430	319.95	4	0	8	✓

Note. — SMC star forming regions: Col. 1 contains the adopted identification name. *A* denotes aggregate, *C* complex, and *SC* super-complex. Cols. 2 and 3 contain the right ascension and declination of the “center” of each star forming region, that are also given in pixels in Cols. 4 and 5. Col. 6 gives the dimension of each star forming region, while Cols. 7, 8, and 9 list the number of associations, SNRs, and HII regions found in each region. Col. 10 list the 8550-MHz flux. Areas that have not been identified due to incomplete coverage of the field of view are marked as ‘n/a’ in the table.

Table 2: List of the derived IRAS fluxes for the SMC star forming regions.

Star forming region	f12	L12	f25	L25	f60	L60	f100	L100	F_{60}/F_{100}	F_{60}
A1	0.11	2.01e+03	1.02	8.97e+03	11.45	4.21e+04	24.26	5.35e+04	0.47	0.06
A2	1.89	4.73e+04	13.20	1.58e+05	59.71	2.98e+05	63.92	1.92e+05	0.93	0.32
A3	0.22	6.41e+03	0.66	9.08e+03	8.75	5.00e+04	21.81	7.48e+04	0.40	0.05
A4	0.34	2.21e+04	2.82	8.70e+04	26.37	3.39e+05	48.40	3.73e+05	0.54	0.14
C1	0.42	8.77e+04	2.37	2.37e+05	24.12	1.00e+06	45.47	1.14e+06	0.53	0.13
C2	0.68	7.20e+04	3.10	1.58e+05	30.68	6.51e+05	57.09	7.27e+05	0.54	0.16
A5	0.40	9.89e+03	4.06	4.87e+04	24.17	1.21e+05	34.62	1.04e+05	0.70	0.13
A6	0.17	5.42e+03	0.88	1.38e+04	13.27	8.66e+04	24.94	9.77e+04	0.53	0.07
A7	0.21	1.35e+04	0.56	1.74e+04	11.76	1.51e+05	23.22	1.79e+05	0.51	0.06
C3	0.34	7.66e+04	1.69	1.82e+05	16.66	7.48e+05	27.76	7.48e+05	0.60	0.09
C4	0.67	5.29e+04	4.06	1.53e+05	29.23	4.59e+05	43.10	4.06e+05	0.68	0.15
C5	0.40	6.89e+04	1.42	1.17e+05	21.77	7.46e+05	40.28	8.28e+05	0.54	0.12
C6	0.29	1.35e+05	0.91	2.05e+05	15.19	1.43e+06	29.79	1.68e+06	0.51	0.08
A8	0.41	1.69e+04	1.27	2.51e+04	17.27	1.43e+05	37.49	1.86e+05	0.46	0.09
A9	0.09	1.73e+03	0.34	2.95e+03	9.68	3.56e+04	19.17	4.22e+04	0.50	0.05
A10	0.14	4.59e+03	0.98	1.54e+04	11.20	7.31e+04	21.63	8.47e+04	0.52	0.06
A11	0.27	6.85e+03	1.39	1.66e+04	14.48	7.24e+04	25.92	7.78e+04	0.56	0.08
C7	0.60	1.50e+05	4.30	5.19e+05	40.93	2.06e+06	55.01	1.66e+06	0.74	0.22
C8	0.22	2.34e+04	1.14	5.86e+04	11.91	2.54e+05	24.17	3.09e+05	0.49	0.06
C9	0.18	8.95e+03	0.82	1.92e+04	13.24	1.30e+05	26.57	1.56e+05	0.50	0.07
A12	0.16	6.65e+03	0.76	1.50e+04	9.83	8.10e+04	22.53	1.11e+05	0.44	0.05
A13	0.20	8.14e+03	0.93	1.85e+04	11.83	9.77e+04	22.14	1.10e+05	0.53	0.06
C10	0.18	2.14e+04	0.54	3.20e+04	11.02	2.70e+05	22.24	3.27e+05	0.50	0.06
C11	0.17	5.23e+04	0.41	5.90e+04	10.09	6.11e+05	20.36	7.40e+05	0.50	0.05
A14	0.24	1.12e+04	0.99	2.19e+04	11.50	1.06e+05	24.49	1.35e+05	0.47	0.06
A15	0.21	1.08e+04	0.68	1.66e+04	14.94	1.52e+05	28.87	1.77e+05	0.52	0.08
SC1	0.17	7.12e+04	0.52	1.01e+05	11.80	9.63e+05	21.09	1.03e+06	0.56	0.06
C12	0.22	9.49e+04	0.51	1.05e+05	11.44	9.81e+05	24.89	1.28e+06	0.46	0.06
A16	0.27	3.22e+04	0.58	3.28e+04	14.62	3.43e+05	31.95	4.50e+05	0.46	0.08
A17	0.16	1.12e+04	0.64	2.12e+04	11.49	1.58e+05	25.41	2.10e+05	0.45	0.06
C13	0.25	2.81e+04	0.61	3.36e+04	14.58	3.35e+05	24.74	3.41e+05	0.59	0.08
C14	0.26	1.37e+04	0.76	1.93e+04	16.25	1.72e+05	32.13	2.05e+05	0.51	0.09
A18	0.05	2.22e+03	0.28	5.56e+03	9.14	7.46e+04	21.86	1.07e+05	0.42	0.05
C15	0.20	1.43e+04	0.81	2.79e+04	19.34	2.76e+05	32.89	2.82e+05	0.59	0.10
A19	0.28	2.02e+04	1.61	5.50e+04	26.82	3.83e+05	39.19	3.36e+05	0.68	0.14
SC2	0.19	9.75e+04	0.91	2.22e+05	20.38	2.08e+06	33.72	2.06e+06	0.60	0.11
C16	0.24	4.81e+04	1.27	1.25e+05	27.76	1.13e+06	43.07	1.05e+06	0.64	0.15
A20	0.09	1.59e+03	0.41	3.63e+03	11.96	4.39e+04	21.41	4.72e+04	0.56	0.06
A21	0.41	2.45e+04	1.04	2.97e+04	16.35	1.95e+05	31.89	2.28e+05	0.51	0.09
C17	0.63	5.29e+04	2.25	9.09e+04	37.99	6.39e+05	67.47	6.82e+05	0.56	0.20
C18	0.80	9.25e+04	2.68	1.49e+05	50.88	1.18e+06	88.26	1.23e+06	0.58	0.27
C19	0.60	2.66e+05	1.91	4.04e+05	37.30	3.29e+06	65.70	3.47e+06	0.57	0.20
C20	1.05	1.09e+05	4.36	2.18e+05	49.94	1.04e+06	83.98	1.05e+06	0.59	0.26
A22	0.34	1.68e+04	0.86	2.01e+04	14.38	1.41e+05	30.15	1.77e+05	0.48	0.08
SC3	0.46	7.29e+05	1.46	1.11e+06	25.93	8.20e+06	47.70	9.05e+06	0.54	0.14
C21	0.65	7.97e+04	2.00	1.18e+05	39.43	9.74e+05	67.38	9.98e+05	0.59	0.21
C22	0.68	4.15e+04	1.59	4.68e+04	29.26	3.58e+05	54.04	3.97e+05	0.54	0.15
A23	0.61	3.77e+04	1.88	5.57e+04	26.61	3.28e+05	53.42	3.96e+05	0.50	0.14
A24	0.35	2.13e+04	1.07	3.13e+04	20.69	2.53e+05	37.33	2.74e+05	0.55	0.11
C23	0.55	7.36e+04	1.76	1.14e+05	26.83	7.23e+05	49.98	8.08e+05	0.54	0.14

Note. — Derived IRAS fluxes (MJy sr^{-1}), luminosities (in units of L_{\odot}) of the identified starforming region at 12, 25, 60, and 100 μm , the flux ratio F_{60}/F_{100} and the flux at 60 μm in Jy per pixel.

Table 3: Estimations of uncertainties for the IRAS fluxes involved in diagrams. Indicative values for 8550 MHz emission are also given.

Star forming region	error Log(F_{60})	error Log(F_{60}/F_{100})	8550 MHz
A1	0.05	0.07	n/a
A2	0.01	0.02	n/a
A3	0.07	0.08	0.00
A4	0.02	0.03	30.85
C1	0.03	0.03	42.60
C2	0.02	0.03	66.63
A5	0.03	0.04	0.00
A6	0.05	0.06	0.00
A7	0.05	0.07	0.52
C3	0.04	0.05	27.70
C4	0.02	0.03	66.56
C5	0.03	0.04	68.71
C6	0.04	0.05	28.67
A8	0.04	0.04	0.23
A9	0.06	0.08	0.00
A10	0.06	0.07	0.00
A11	0.04	0.06	0.00
C7	0.02	0.02	148.33
C8	0.05	0.07	0.00
C9	0.05	0.06	0.00
A12	0.06	0.08	0.00
A13	0.05	0.07	0.00
C10	0.06	0.07	0.00
C11	0.06	0.08	0.00
A14	0.05	0.07	0.00
A15	0.04	0.05	0.00
SC1	0.05	0.07	0.05
C12	0.05	0.07	0.00
A16	0.04	0.05	0.00
A17	0.05	0.07	0.00
C13	0.04	0.06	0.00
C14	0.04	0.05	0.00
A18	0.07	0.08	0.00
C15	0.03	0.04	0.00
A19	0.02	0.04	48.39
SC2	0.03	0.04	8.72
C16	0.02	0.03	12.95
A20	0.05	0.07	0.00
A21	0.04	0.05	1.31
C17	0.02	0.02	15.78
C18	0.01	0.02	73.83
C19	0.02	0.02	43.19
C20	0.01	0.02	56.32
A22	0.04	0.05	0.00
SC3	0.02	0.03	16.29
C21	0.02	0.02	72.48
C22	0.02	0.03	0.00
A23	0.02	0.03	0.46
A24	0.03	0.04	12.14
C23	0.02	0.03	0.52

Note. — SMC star forming regions: Col. 1 contains the adopted identification name. Cols. 2 and 3 contain errors for Log(F_{60}) and Log($60/100$), while Col. 4 gives the 8550 MHz emission.

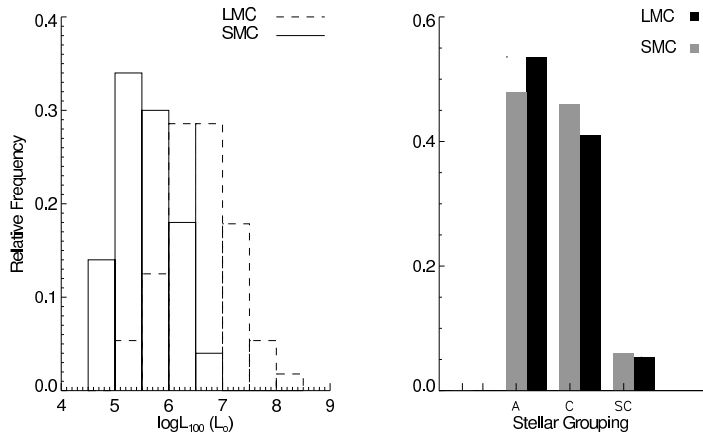


Fig. 4.— Relative frequency distribution of star forming regions with respect to their 100 μm -luminosity, in units of L_{\odot} (left) and relative frequency distribution of the three kinds of star forming regions (right) for LMC and SMC.

REFERENCES

- Bica E. L. D., & Schmitt H. R. 1995, *ApJS*, 101, 41
- Bontekoe Tj. R., Kester D. J. M., Stanimirović S., Staveley-Smith L., & van der Hulst J. M, 1999, *IAU Symposium*, Vol. 190, Edited by Y.-H. Chu, N. Suntzeff, J. Hesser, & D. Bohlender, p. 122
- Bontekoe Tj. R., Koper E., & Kester D. J. M. 1994, *A&A*, 284, 1037
- Efremov Yu. N. 2004, *astro-ph/0410702*
- Efremov Yu. N., & Elmegreen B. G. 1998, *MNRAS*, 299, 588
- Gardiner L. T., & Noguchi M. 1996, *MNRAS*, 278, 191
- Hatzidimitriou D., & Hawkins M. R. S. 1989, *MNRAS*, 241, 667
- Haynes R. F., Murray J. D., Klein U., & Wielebinski R. 1986, *A&A*, 159, 22
- Helou G., Khan I. R., Malek L., & Boehmer L. 1988, *ApJS*, 68, 151
- Lehnert M. D., & Heckman T. M. 1995, *ApJS*, 97, 89
- Livanou E., Kontizas M., Gonidakis I., Kontizas E., Maragoudaki F., Oliver S., Efstathiou A., & Klein U. 2006, *A&A*, 451, 431
- Lonsdale C.J., Helou G., Good J.C., & Rice W. 1985, *Catalogued Galaxies and Quasars Observed in the IRAS Survey* (Pasadena:JPL)
- Maragoudaki F., Kontizas M., Kontizas E., Dapergolas A., & Morgan D. H. 1998, *A&A*, 338, 29
- Maragoudaki F., Kontizas M., Morgan D. H., Kontizas E., Dapergolas A., & Livanou E. 2001, *A&A*, 379, 864
- Mathewson D. S., Ford V. L., & Visvanathan N. 1988, *ApJ*, 333, 617
- Rice W., Lonsdale C. J., Soifer B .T., Neugebauer G., Koplan E. L., Lloyd L. A., de Jong T., & Habing H. J. 1988, *ApJS*, 68, 91
- Yoshizawa A., & Noguchi M. 2003, *MNRAS*, 339, 1135